Journal of Power Sources 196 (2011) 6394–6399

Contents lists available at ScienceDirect

Journal of Power Sources

journal homepage: www.elsevier.com/locate/jpowsour

Facile synthesis and electrochemical characterization of porous and dense TiO_2 nanospheres for lithium-ion battery applications

Hong-En Wang[a,b], Hua Cheng[a,c], Chaoping Liu[a,b], Xue Chen[b], Qinglai Jiang[c], Zhouguang Lu[a,c], Yang Yang Li[a], C.Y. Chung[a], Wenjun Zhang[a,b], Juan Antonio Zapien[a,b,*], Ludvik Martinu[a,d], Igor Bello[a,b,*]

[a] Department of Physics and Materials Science, City University of Hong Kong, Hong Kong SAR, PR China
[b] Center of Super-Diamond and Advanced Films (COSDAF), City University of Hong Kong, Hong Kong SAR, PR China
[c] College of Chemistry and Chemical Engineering, Central South University, Changsha, PR China
[d] On Leave from the Department of Engineering, Ecole Polytechnique, Montreal, Quebec, Canada

ARTICLE INFO

Article history:
Received 13 December 2010
Received in revised form 18 March 2011
Accepted 29 March 2011
Available online 5 April 2011

Keywords:
Titanium dioxide
Nanosphere
Lithium-ion battery
Nanoporous material

ABSTRACT

We present a two-step method to optimize the nanoporous characteristics of TiO_2 samples thus enabling a higher charge and discharge capacity and a larger rate capability compared to dense TiO_2 materials. We use a simple sol–gel process to fabricate spherical titanium glycolates precursors followed by subsequent hydrothermal or annealing treatments resulting, respectively, in highly porous or dense TiO_2 nanospheres. These processes enable control of the grain size, pore structure, and specific surface area of the TiO_2. The fabricated TiO_2 nanostructures have been subsequently used to assemble lithium-ion batteries. Galvanostatic discharge–charge tests indicate that the porous TiO_2 nanospheres possess high and stable reversible capacity of 229, 133, and 56 mAh g^{-1} at 0.06, 0.6 and 6 C, respectively; whereas the corresponding values for dense TiO_2 nanospheres are 217, 45, and ~1 mAh g^{-1}. Such considerable improvement of the electrochemical activity is attributed to the porous TiO_2 nanostructures, and subsequent change in diffusion length, and enables the possibility to optimize the high rate capability in TiO_2-based lithium-ion batteries.

1. Introduction

TiO_2 is an important multifunctional wide bandgap semiconductor with excellent physical properties, chemical stability, environmental compatibility, and low production cost. TiO_2 offers a broad range of applications such as photocatalysis [1], water splitting [2], dye-sensitized solar cells [3] and quantum-dots sensitized solar cells [4]. Recently, TiO_2 has also been intensively investigated as a promising anode material for lithium-ion batteries (LIBs) due to its high storage ability of lithium ions (Li^+), very high rate capability, and operation safety during charge–discharge cycling [5–12]. TiO_2 nanomaterials with variable polymorphs, morphologies and pore structures, such as nanocrystals, one-dimensional (1D) nanostructures, and porous nanostructures, have been synthesized by a variety of physical and chemical methods, and they were evaluated as electrode materials for LIBs [13].

Among such nanostructures, TiO_2 nanocrystals have been mostly studied because their high specific surface area can provide more active sites for surface and interface reactions [3,14]. However, TiO_2 nanocrystals agglomerate easily, and they are difficult to be separated and purified in both the preparation and recovery processes. In addition, conventional hydrothermal synthesis of TiO_2 nanocrystals from Ti^{4+} sols usually requires high hydrothermal temperatures (>200 °C), and thus the use of special facilities and safety precautions. Therefore, assembly of TiO_2 nanocrystals into large microstructures with porous networks, or direct synthesis of porous nanostructures, becomes a technical challenge. A commercially viable electrode material should possess microstructures which can be easily synthesized, purified and used in the different applications without significant loss of their large specific surface area.

Several methods have been proposed to prepare porous TiO_2 nanostructures. Eiden-Assmann and Widoniak [15] synthesized porous TiO_2 spherical particles by sol–gel method with the assistance of polymer additives. Yang et al. [16] obtained cauliflower-like mesoporous TiO_2 spheres using block copolymers as structural directing agents. Li and Zeng [17] synthesized hollow Sn-doped TiO_2 nanospheres using TiF_4 as a precursor. Jung et al. [18] prepared F-doped mesoporous anatase TiO_2 by a hydrother-

* Corresponding authors at: Department of Physics and Materials Science and Center of Super-Diamond and Advanced Films, City University of Hong Kong, Hong Kong SAR, PR China. Tel.: +852 3442 7823; fax: +852 3442 0547.
E-mail addresses: apjazs@cityu.edu.hk (J.A. Zapien), apibello@cityu.edu.hk (I. Bello).

0378-7753/$ – see front matter © 2011 Elsevier B.V. All rights reserved.
doi:10.1016/j.jpowsour.2011.03.085

mal method with the aid of urea. Guo and Hu [19] used TiO_2–$CdSO_4$ composites as an intermediate to prepare hierarchical mesoporous TiO_2 submicron-size spheres. Zhong et al. [20] acquired nanoporous TiO_2 spheres by a reflux method. Rossmanith et al. [21] prepared porous anatase TiO_2 nanoparticles by a combined sol–gel and mini emulsion technique. Yue et al. [22] used mesoporous silicas as hard templates to synthesize mesoporous monocrystalline TiO_2. Chen et al. [23] prepared ordered arrays of mesoporous TiO_2 spheres through patterned triblock copolymer as templates.

In general, direct synthesis of porous TiO_2 nanostructures under mild reaction conditions without using any templates or additives is still difficult. Additional problem is the fact that titanium alkoxides precursors tend to hydrolyze in the presence of traces of moisture. To prevent such hydrolyses of titanium alkoxides acids are usually used. Ethylene glycol (EG) is another popular alternative to stabilize titanium alkoxides precursors by the chain exchange reactions. Jiang et al. [24] proposed a route for the synthesis of monodispersed spherical TiO_2 colloids by an EG-mediated sol–gel method. Other processes based on this approach have also been reported [25–27]. However, only dense TiO_2 spheres have been obtained by the subsequent annealing processes.

In the present work, we propose a simple two-step process to synthesize both porous and solid anatase TiO_2 nanospheres. Firstly, colloid titanium glycolate (TEG) precursor spheres are obtained by a modified sol–gel technique. Secondly, porous TiO_2 nanospheres are synthesized by low-temperature hydrothermal crystallization, while dense TiO_2 nanospheres are obtained by directly annealing the TEGs. We have demonstrated the successful implementation of the prepared porous and dense TiO_2 nanospheres as anodes in LIBs, and have established the correlation between different electrochemical performances and their distinct structural characteristics.

2. Experimental

Tetrabutyl titanate (TBT, 97%), ethylene glycol (EG, ≥99%), acetone (≥99.9%) and ethanol (≥99.5%) from Sigma–Aldrich were used without further purification.

In a typical procedure, 1 mL TBT was added to 20 mL EG under magnetic stirring. The mixture was continuously stirred for several hours until a transparent sol was obtained. Subsequently, the sol was poured into 80 mL acetone containing 1 mL of distilled water under vigorous stirring. This mixing resulted in a white precipitate. After stirring for another 1 h and ageing for 12 h, the white precipitates were collected by centrifugation, followed by repeatedly rinsing with ethanol, acetone and distilled water in sequence and finally dried in an oven at 60 °C for 12 h.

For the synthesis of porous TiO_2 nanospheres, the TEG precursors were dispersed into 200 mL distilled water and subjected to hydrothermal treatment at 90–100 °C for 4–15 h. Subsequently, white precipitates were obtained by centrifugation. These precipitates were also rinsed and then dried at 60 °C for 12 h.

For the preparation of dense TiO_2 nanospheres, the TEG precursors were annealed in air at 450 °C for 2 h with a ramping heating rate of 5 °C min^{-1}, followed by natural cooling in ambient.

Crystal structures of the samples were examined by x-ray diffraction (XRD) using a Siemens D500 diffractometer operated at 40 kV and 30 mA. The morphologies were observed with a Philips XL30 FEG field-emission scanning electron microscope (FESEM) and a Philips CM20 transmission electron microscope (TEM). High-resolution TEM (HRTEM) analysis was performed using a Philips CM200 FEG TEM operating at 200 kV.

Specific surface area and pore size distribution of the samples were determined by nitrogen adsorption–desorption isotherms at 77 K using a NOVA 1200e Surface Area & Pore Size Analyzer (Quantachrome Instruments). Prior to adsorption experiments, the samples were degassed at 150 °C for 2 h.

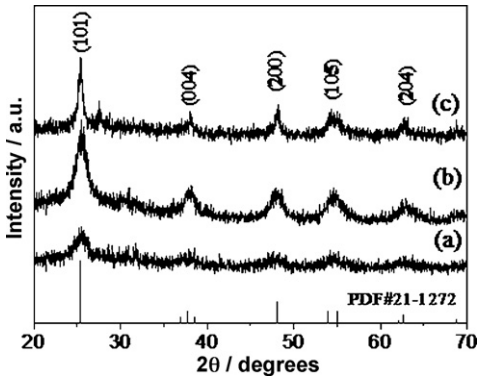

Fig. 1. XRD patterns of TiO_2 samples synthesized at different conditions. (a and b) TiO_2 structures obtained by hydrothermal synthesis using precursors of titanium glycolates at 90 °C for 4 h and 100 °C for 15 h, respectively; (c) annealing the titanium glycolates at 450 °C for 2 h.

Electrochemical characterization was performed in the form of coin type cells. The working electrodes were prepared by shock-milling of a powder mixture containing 80 wt.% active materials (TiO_2), 10 wt.% carbon black and 10 wt.% polyvinylidene difluoride (PVDF) dispersed in acetone. The cells were assembled in an argon-filled glove-box. A typical coin cell consisted of a lithium foil as the counter electrode and reference electrode, 10 mg working electrode, one sheet of glass fiber disk and one layer of Celgard 2025 (Celgard, Inc., USA) as the separators, and, finally, 1 M $LiPF_6$ dissolved in ethylene carbonate (EC) and dimethyl carbonate (DMC) mixture (1:1, w/w) as electrolyte. Galvanostatic charge–discharge experiments were carried out with an Arbin Instruments (BT 200, College Station, TX) system cycled between 1 and 3 V (Li^+/Li) at room temperature. The maximum Li insertion into TiO_2 was assumed to be 0.5 (~167.5 mAh g^{-1}), and thus the discharge and charge rates were based on the following relationship: 1 C = 167.5 mA g^{-1}.

3. Results and discussion

In the first part of this work, we study the microstructure of the synthesized TiO_2 nanospheres. Fig. 1 shows XRD patterns of TiO_2 samples synthesized at different experimental conditions. Clearly, all the prepared samples exhibit pure anatase structures (PDF#21-1272). The broad diffraction peaks shown in Fig. 1(a) indicate that the TiO_2 product after hydrothermal crystallization at 90 °C for 4 h is weakly crystalline. However, after hydrothermal treatment at 100 °C for 15 h, the crystallinity of the TiO_2 is substantially improved (Fig. 1(b)). The full width at half maximum (FWHM) of the peak at two theta of 25.3° is reduced from 1.8° (Fig. 1(a)) to 1.4° (Fig. 1(b)), a value characteristic for all the remaining peaks. Compared to the TiO_2 samples obtained by hydrothermal treatment, the diffraction peaks of the TiO_2 product synthesized by annealing are even sharper. The FWHM of the peak at two theta of 25.3° is 0.6° (Fig. 1(c)), suggesting the presence of crystallites with larger sizes.

The microstructure of the TiO_2 products has further been analyzed by electron microscopies. The FESEM images in Fig. 2(a) reveal that the TEG precursors are composed of spherical particles with smooth surfaces, and diameters from 60 to 120 nm. After hydrothermal treatment of the precursor solution at 90 °C for 12 h or 100 °C for 15 h, the surfaces of the TiO_2 particles become coarse as shown in Fig. 2(b and c), respectively. In contrast to the hydrothermal treatment, the surface of the TiO_2 spheres prepared by annealing at 450 °C for 2 h (Fig. 2(d)) remains smooth. The spheres are slightly smaller than the TEG precursors and some tend to aggregate into larger particles.

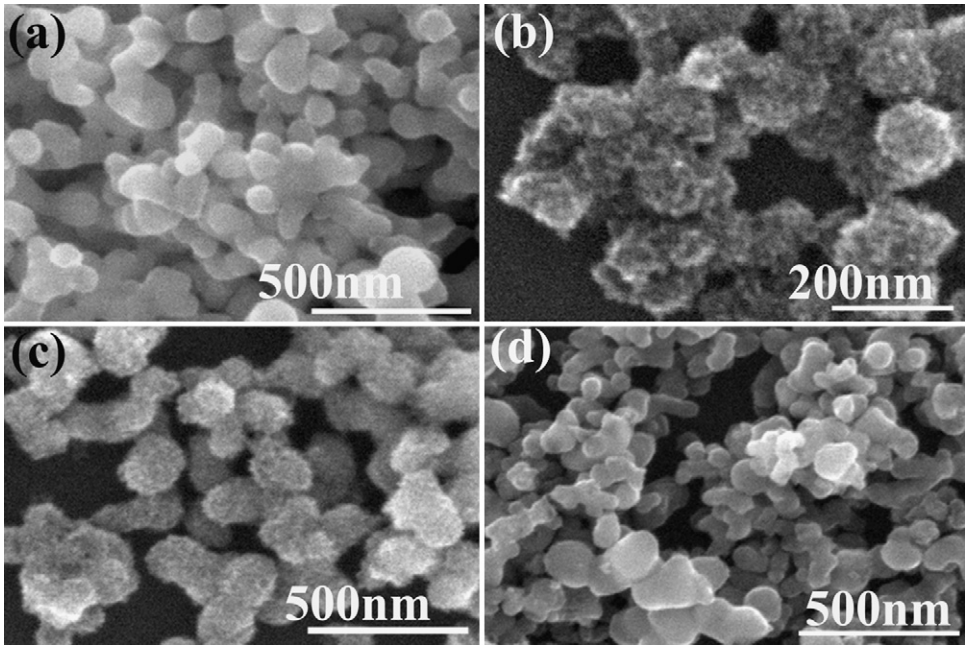

Fig. 2. SEM images of (a) titanium glycolate precursors; (b and c), the TiO_2 products obtained by hydrothermal treatment of titanium glycolates at 90 °C for 12 h and 100 °C for 15 h, respectively; (d) TiO_2 structure prepared by annealing titanium glycolates at 450 °C for 2 h.

Bright field TEM and HRTEM images as well as SAED patterns provide additional details on the TiO_2 spheres synthesized by hydrothermal treatment of the TEG precursors at 90 °C for 12 h (Fig. 3). The TEM image in Fig. 3(a) indicates that the TiO_2 product consists of spherical particles with sizes similar to those of the TEG precursors. The SAED pattern in Fig. 3(b) shows the diffraction pattern is composed of concentric circles, revealing polycrystalline nature of the TiO_2 particles. Complementary energy-dispersive X-ray (EDX) spectra (not shown here) infer the presence of only four elements, namely, Cu, C, Ti, and O. Here, Cu and C originate

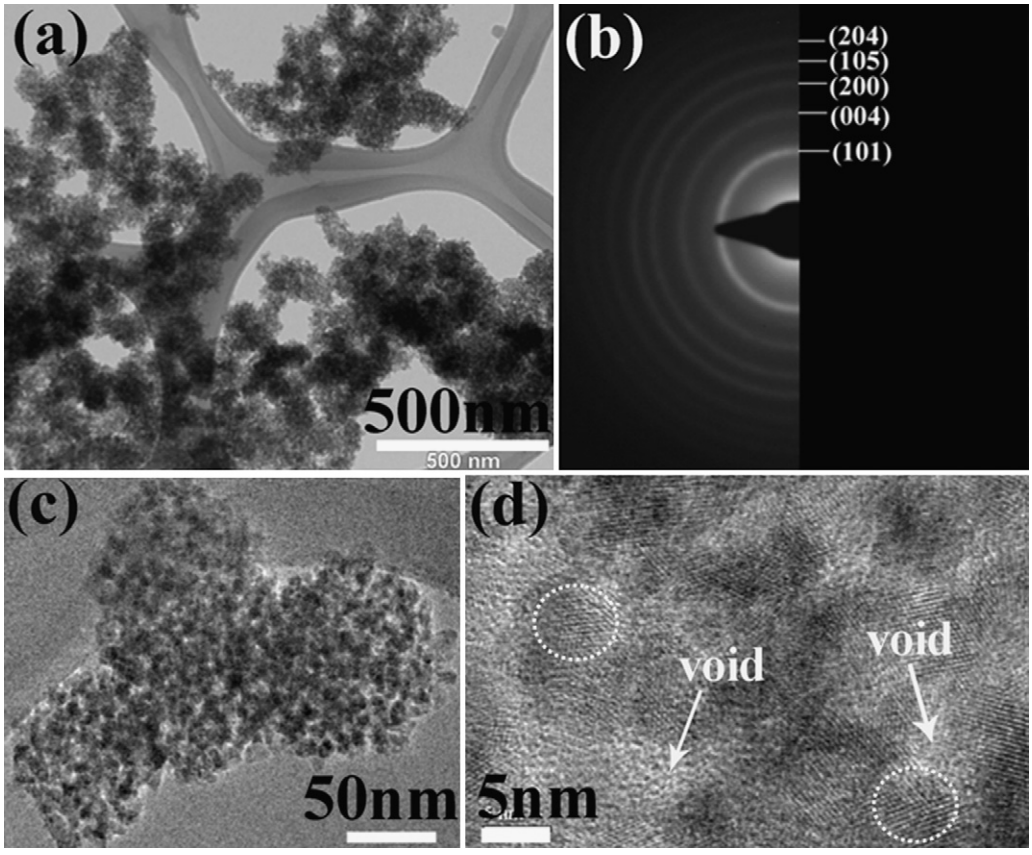

Fig. 3. (a) Bright field TEM image; (b) SAED pattern; (c) high-magnification TEM image; and (d) HRTEM image of porous TiO_2 nanospheres synthesized by hydrothermal treatment of titanium glycolates at 90 °C for 12 h (the dotted circles indicate the TiO_2 nanocrystals).

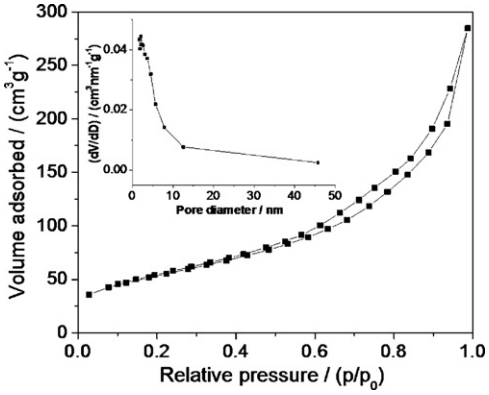

Fig. 4. Nitrogen adsorption–desorption isotherms and pore size distribution (in inset) of porous TiO_2 nanospheres synthesized by hydrothermal treatment of titanium glycolates at 90 °C for 12 h.

from the copper grid coated with a carbon film, while Ti and O are constituent's characteristic of the synthesized product with a Ti/O atomic ratio of 1:2. Fig. 3(c and d) reveals that each single TiO_2 sphere possesses a porous structure, and consists of small nanocrystals with a crystallite size of ~5 nm. This product differs considerably from the TiO_2 dense structure prepared by the annealing process [24].

In the second part of this work, we studied the effects related to the enhanced specific surface area. The nitrogen adsorption/desorption isotherms of the porous TiO_2 nanospheres can be identified as type IV, which are typical characteristics of mesoporous materials (Fig. 4). The corresponding Brunauer–Emmett–Teller (BET) specific surface area of the TiO_2 spheres was found to yield ~64 $m^2 g^{-1}$. The Barrett–Joyner–Halenda (BJH) pore size distribution (inset image in Fig. 4) indicates that the product exhibits pores with sizes typically ranging from 1.7 to 12 nm. In contrast, the BET specific surface areas of TEG precursors and the dense TiO_2 spheres prepared by annealing are ~6.5 and ~15 $m^2 g^{-1}$, respectively, which are much smaller than that of the porous TiO_2 nanospheres synthesized by hydrothermal treatment.

It is well known that titanium alkoxides are usually very reactive with water, and white precipitates are slowly produced when they are exposed to moisture. EG can be effectively used as a chelating reagent to stabilize titanium alkoxide by a chain exchange reaction as follows:

$$Ti(OR)_4 + 2HO(CH_2)_2OH \rightarrow Ti(O(CH_2)_2O)_2 + 4ROH, \quad (1)$$

where "R" stands for an alkyl group.

The resulting TEGs are very stable and can even be stored for a long time without observing obvious precipitates. After pouring them into an acetone bath containing a small amount of water, spherical TEG can be precipitated because of their insolubility in acetone. The particle size and size distribution can be finely tuned by altering the reactants concentrations as described elsewhere [25]. In the current experiments, it is noticed that two types of structures, i.e., porous or dense, can be obtained by simply changing the post-treatment processes. It is believed that this structural disparity is caused by differences in the reaction environments.

During the hydrothermal process, the TEG precursor spheres may be attacked by water, the adsorbed EG molecules would be substituted gradually and simultaneously the outer surface of the precursor may crystallize. This crystallization would stabilize the TiO_2 surface structure and thus prevent its collapse. In addition, the water molecules can penetrate inside the TEG precursors to substitute the EG molecules, resulting in porous spheres. On the other hand, during the annealing process in air, the TEG precursors would directly decompose into TiO_2 and CO_2 along with the elevation of annealing temperatures. This quick decomposition of organics from the entire TEG precursors would induce contraction of TiO_2 in order to reduce their surface energy. As a result, a dense spherical structure is obtained [24].

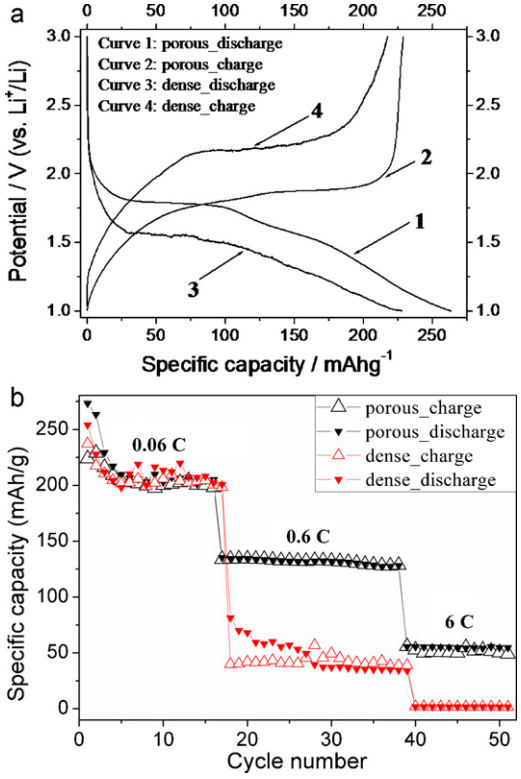

Fig. 5. (a) Discharge–charge curves of the porous and dense TiO_2 nanospheres synthesized by hydrothermal treatment of titanium glycolates at 90 °C for 12 h and annealing titanium glycolates at 450 °C for 2 h, respectively. (b) Cycle performances of the porous and dense TiO_2 nanospheres synthesized by hydrothermal treatment of titanium glycolates at 90 °C for 12 h and annealing titanium glycolates at 450 °C for 2 h, respectively.

In the third part of this work, we studied the electrochemical performances of TiO_2 nanospheres in the LIBs. Li^+ insertion/extraction into/from TiO_2 matrix during the electrochemical discharge/charge processes can be described by the following equation:

$$TiO_2 + x(Li^+ + e) = Li_xTiO_2 \quad (0 \le x \le 1). \quad (2)$$

Theoretically, the highest Li-storage capacity (~335 mAh g^{-1}) corresponds to the insertion of one Li per TiO_2 inducing a complete reduction of Ti^{4+} into Ti^{3+} [6]. From a practical viewpoint, reversible Li insertion into anatase TiO_2 is about 0.6 (~200 mAh g^{-1}) at 1.78 V versus Li^+/Li at a low discharge rate.

Fig. 5 shows the discharge-charge curves of the synthesized TiO_2 samples in LIBs. The porous TiO_2 nanospheres display well developed discharge–charge characteristics in Fig. 5(a). The discharge and charge plateaus of porous TiO_2 nanospheres are located at ~1.78 and ~1.88 V, respectively. The discharge curve of porous TiO_2 nanospheres can be divided into three domains. The first domain is the monotonous potential drop, which is induced by a solid solution insertion mechanism linked to small particle and crystalline sizes [28]. The second domain with constant potential at ~1.78 V relates to Li^+ insertion into the interstitial octahedral site of TiO_2, during which a two-phase reaction occurs with phase equilibrium of Li-poor $Li_{0.01}TiO_2$ (tetragonal) and Li-rich $Li_{0.6}TiO_2$ (orthorhombic) [29]. The third domain is a sloped potential associated with Li storage in the surface as well as the formation of Li_1TiO_2 phase

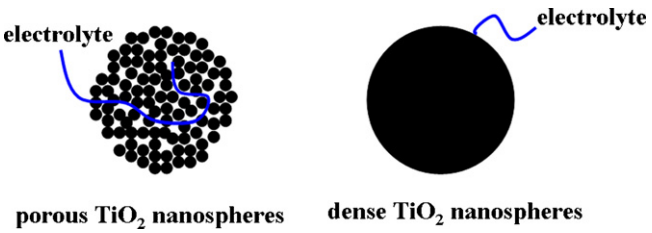

Fig. 6. Schematic diagram of the porous and dense TiO_2 nanospheres used in lithium-ion batteries.

[30]. The initial discharge and charge capacities of the porous TiO_2 nanospheres at 0.06 C are ~263 and ~229 mAh g^{-1}, respectively.

Dense TiO_2 nanospheres show similar discharge and charge behavior compared to porous TiO_2. However, they display a relatively lower discharge plateau (~1.55 V) and a higher charge plateau (~2.15 V), suggesting a more pronounced polarization behavior during the electrochemical discharge–charge processes. The discharge and charge capacities of the dense TiO_2 nanospheres at 0.06 C are ~228 and ~217 mAh g^{-1}, respectively, which are slightly lower than those of the porous TiO_2 nanospheres.

For comparison, Fig. 5(b) shows the cyclic performance of the two kinds of TiO_2 samples under different rates. The porous TiO_2 nanospheres exhibit high initial discharge and charge capacities and a slight capacity drop during the first three discharge–charge cycles. The main reason for the capacity drop during the first a few discharge/charge cycles is that a small part of the insertion/extraction of Li^+ into/from TiO_2 nanospheres is irreversible. This irreversibility should be related to the size, morphology, crystallinity, porous characteristics of our synthesized samples. In addition, some parasitic effects proceeding at potentials close to the cut-off might also account for part of the capacity drop. Due to the low current rate and long time of discharge/charge, the system is kept for a long time either at lower potentials (~1 V), where the reduction of electrolyte Li^+ ions and the formation of dendrites may take place, or at higher potentials (~3 V), where impurities in an electrolyte including adsorbed water are oxidized. To overcome this effect, a narrow potential window (1.3–2.5 V) can be adopted. Thereafter, the porous nanospheres show highly stabilized discharge and charge capacities of ~200 mAh g^{-1} at 0.06 C. When the discharge-charge rate is increased to 0.6 C, the discharge and charge capacities are reduced to 133 mAh g^{-1}. The capacities retain a value of 56 mAh g^{-1} when the rate is further increased to 6 C.

The dense TiO_2 nanospheres show a similar reversible capacity as found for the porous TiO_2 nanospheres at a low rate (0.06 C). However, at high rate, the dense nanospheres display a much lower electrochemical capacity compared to porous TiO_2. The capacities of the dense samples are found to be ~45 mAh g^{-1} at 0.6 C, which represents about 34% of the value for the porous material. If the rate is further increased to 6 C, the dense samples almost completely lose their Li^+ storage ability (~1 mAh g^{-1}). These results indicate that the porous TiO_2 nanospheres have a much larger rate capability than the dense TiO_2 nanospheres.

The different electrochemical characteristics of the two types of samples can be ascribed to their fairly distinct geometries. The discharge/charge processes involve the Li^+ insertion/extraction into/from the TiO_2 crystals and their diffusion in the TiO_2 matrix. Fig. 6 gives the schematic diagrams of these two kinds of TiO_2 nanospheres during the electrochemical discharge/charge reactions (only one single porous and dense nanospheres were illustrated for convenience). From Fig. 6, several advantages of the porous TiO_2 nanospheres can be clearly observed. Firstly, their porous structure significantly increases the specific surface area (which is 4-fold of that of the dense counterparts). Secondly, their interconnected pore channels improve the wettability of the electrolyte and increase the contact interfaces between the TiO_2 active materials and the electrolyte while shorten the Li^+ diffusion length. These factors facilitate fast Li^+ ion transport and electrochemical reaction dynamics. In addition, the porous structure may also alleviate the volume change of TiO_2 matrix during the Li^+ insertion/extraction processes. Consequently, high reversible electrochemical capacity and rate capability can be achieved. In contrast to the porous structure, the dense TiO_2 nanospheres possess a considerably smaller specific surface area and thus smaller contact interface with the electrolyte. Moreover, the Li^+ diffusion length in the dense TiO_2 matrix is much longer than that in the porous TiO_2 matrix. When a very high rate is used, most of the charges probably accumulated on the particle surface, and as a result, a large portion of the electrode became inactive.

4. Conclusions

In conclusion, porous and dense TiO_2 nanospheres have been synthesized via a simple sol–gel process followed by subsequent hydrothermal or annealing treatments, respectively. Electrochemical tests in lithium-ion batteries demonstrated that the porous TiO_2 samples possess a higher discharge capacity and better rate capability than the dense TiO_2 materials. Such considerable improvement of the electrochemical activity is believed to be caused by such unique porous structures that favor electrochemical reactions. The electrochemical performances of the porous TiO_2 nanostructures may be further improved by optimizing their structural parameters, such as particle size, pore size, morphology, crystallinity via altering experimental conditions. In addition, the as-synthesized porous and dense TiO_2 nanospheres may also find possible applications in other fields, such as dye- and/or quantum dot-sensitized solar cells, photocatalysis, etc.

Acknowledgement

This work was fully supported by GRF of Hong Kong under the project number CityU 110 209.

References

[1] Z.B. Zhang, C.C. Wang, R. Zakaria, J.Y. Ying, J. Phys. Chem. B 102 (1998) 10871.
[2] A. Fujishima, K. Honda, Nature 238 (1972) 37.
[3] B. O'Regan, M. Gratzel, Nature 353 (1991) 737.
[4] G.Y. Lan, Z. Yang, Y.W. Lin, Z.H. Lin, H.Y. Liao, H.T. Chang, J. Mater. Chem. 19 (2009) 2349.
[5] H.T. Fang, M. Liu, D.W. Wang, T. Sun, D.S. Guan, F. Li, J. Zhou, T.K. Sham, H.M. Cheng, Nanotechnology 20 (2009) 225701.
[6] P. Kubiak, M. Pfanzelt, J. Geserick, U. Hormann, N. Husing, U. Kaiser, M. Wohlfahrt-Mehrens, J. Power Sources 194 (2009) 1099.
[7] Y. Li, X. Lv, J.H. Li, Appl. Phys. Lett. 95 (2009) 113102.
[8] V. Subramanian, A. Karki, K.I. Gnanasekar, F.P. Eddy, B. Rambabu, J. Power Sources 159 (2006) 186.
[9] D. Wang, D. Choi, Z. Yang, V.V. Viswanathan, Z. Nie, C. Wang, Y. Song, J.G. Zhang, J. Liu, Chem. Mater. 20 (2008) 3435.
[10] D. Dambournet, I. Belharouak, K. Amine, Chem. Mater. 22 (2010) 1173.
[11] J.S. Chen, X.W. Lou, J. Power Sources 195 (2010) 2905.
[12] D. Liu, P. Xiao, Y. Zhang, B.B. Garcia, Q. Zhang, Q. Guo, R. Champion, G. Cao, J. Phys. Chem. C 112 (2008) 11175.
[13] X. Chen, S.S. Mao, Chem. Rev. 107 (2007) 2891.
[14] C.J. Barbe, F. Arendse, P. Comte, M. Jirousek, F. Lenzmann, V. Shklover, M. Gratzel, J. Am. Ceram. Soc. 80 (1997) 3157.
[15] S. Eiden-Assmann, J. Widoniak, Chem. Mater. 16 (2004) 6.
[16] L. Yang, Y. Lin, J. Jia, X. Li, X. Xiao, X. Zhou, Micro. Meso. Mater. 112 (2008) 45.
[17] J. Li, H.C. Zeng, J. Am. Chem. Soc. 129 (2007) 15839.
[18] H.G. Jung, C.S. Yoon, J. Prakash, Y.K. Sun, J. Phys. Chem. C 113 (2009) 21258.
[19] Y.G. Guo, Y.S. Hu, Chem. Commun. (2006) 2783.
[20] L.S. Zhong, J.S. Hu, L.J. Wan, W.G. Song, Chem. Commun. (2008) 1184.
[21] R. Rossmanith, C.K. Weiss, J. Geserick, N. Husing, U. Hormann, U. Kaiser, K. Landfester, Chem. Mater. 20 (2008) 5768.
[22] W. Yue, X. Xu, J.T.S. Irvine, P.S. Attidekou, C. Liu, H. He, D. Zhao, W. Zhou, Chem. Mater. 21 (2009) 2540.

[23] J. Chen, Z. Hua, Y. Yan, A.A. Zakhidov, R.H. Baughman, L. Xu, Chem. Commun. 46 (2010) 1872.
[24] X. Jiang, T. Herricks, Y.N. Xia, Adv. Mater. 15 (2003) 1205.
[25] M. Pal, J.G. Serrano, P. Santiago, U. Pal, J. Phys. Chem. C 111 (2007) 96.
[26] H.K. Yu, G.R. Yi, J.H. Kang, Y.S. Cho, V.N. Manoharan, D.J. Pine, S.M. Yang, Chem. Mater. 20 (2008) 2704.
[27] H. Wang, B. Li, Z.X. Yan, Z.G. Lu, R.J. Cheng, D. Qian, Rare Metals 27 (2008) 1.
[28] G. Sudant, E. Baudrin, D. Larcher, J.M. Tarascon, J. Mater. Chem. 15 (2005) 1263.
[29] M. Wagemaker, A.P.M. Kentgens, F.M. Mulder, Nature 418 (2002) 397.
[30] M. Wagemaker, W.J.H. Borghols, F.M. Mulder, J. Am. Chem. Soc. 129 (2007) 4323.